Discover Applied Sciences

Research

The communication and measurement architecture of BDS-3 global operations and services

Gang Li[1] · Shuren Guo[1] · Wenbin Gong[2] · Kai Han[2] · Weiguang Gao[1] · Fengwei Shao[2] · Wenbin Wang[3] · Chengpan Tang[3] · Feng Zhang[4]

Received: 16 October 2023 / Accepted: 18 March 2024
Published online: 02 April 2024

Abstract
This study introduces the third-generation BeiDou Navigation Satellite System (BDS-3) system's creative global operation and service architecture based on regional stations and Ka-band inter-satellite links (ISLs). The architecture's contributions to BDS-3 include not only combined orbit determination and time synchronization but also autonomous orbit determination and time synchronization, global operations and services. The BDS-3 on-orbit operation results are being presented in the paper to verify the designed capabilities. Compared with BDS-2, the orbit determination accuracy is improving from 0.6 m to 0.15 m, and the time synchronization accuracy is improving from 6.67 ns to 1.16 ns. Under autonomous orbit determination and time synchronization, the 30-day orbit maintenance accuracy reaches 16 m, and the time synchronization accuracy reaches 3.74 ns. The success rate of data transmission reaches 99%, and the delay is better than 12.9 s. In the future, laser ISLs will be used to enhance the system structure and further improve global operation and service capabilities.

Highlights

1. The innovative BDS-3 structure can solve the global service problem even when there are only regional ground stations.
2. Verifies the superior performance of the BDS-3 system based on Ka-band inter-satellite links.
3. Forecasts the technological development trend of the next generation BDS based on laser inter-satellite links.

Keywords BDS-3 · Architecture · Measurement · Communication · Inter-satellite links

1 Introduction

BDS-2 is a regional navigation satellite system, and its space segment is mainly composed of Geostationary Earth Orbit (GEO) and Inclined GeoSynchronous Orbit (IGSO) satellites. These satellites are visible all the time to regional ground stations. BDS-3 space segment consists of 30 satellites, and mainly adopts Medium Earth Orbit (MEO) satellites to provide global services. Under conditions of regional ground stations, the observation arc of global MEO satellites is short,

✉ Gang Li, ligang8212@126.com | [1]Beijing Institute of Tracking and Telecommunication Technology, Beijing 100094, China. [2]Innovation Academy for Microsatellites, Chinese Academy of Sciences, Shanghai 201304, China. [3]Shanghai Astronomical Observatorys, Chinese Academy of Sciences, Shanghai 200030, China. [4]State Key Laboratory of Astronautic Dynamics, Xi'an 710043, China.

making it hard to determine high-precision orbit and clock parameters to support basic RNSS service. It is also almost impossible to control and manage the global MEO satellites effectively.

A typical method is to build worldwide ground stations to supplement the observation arc of global MEO satellites. GPS, GLONASS, and Galileo all adopt the method [1–5]. Taking GPS as an example, the GPS ground control segment consists of six monitor stations and four ground antennas. Those stations and antennas are globally distributed and located near the equator to maximize the tracking arc of MEO satellites. Monitor stations perform the navigation tracking function, while ground antennas perform the satellite commanding and data transmission function. However, the complexity of the operation and maintenance of worldwide ground stations is relatively high. In addition, GPS and GLONASS have realized UHF-band and S-band ISLs respectively [6–9]. The Galileo system does not have ISL capabilities, but it plans to use laser ISLs to improve system performance in the future [10, 11]. And ISL is an additional function for both GPS, GLONASS and Galileo.

BDS-3 has creatively built a new global operations and services architecture with regional ground stations and a Ka-band ISL network to solve the problem. ISLs of navigation satellite systems are a measurement and communication network established between satellites. The architecture uses satellite-ground link and ISL to achieve high-precision orbit determination and time synchronization and provide global RNSS service. Besides, the architecture is required to implement additional functions, including global satellites management, global short message communication, international search and rescue return link service, and autonomous orbit determination and time synchronization. The new architecture has dramatically reduced the demand for global stations and improved the efficiency of system management.

The functions of the proposed architecture are mainly reflected in the following three aspects. Firstly, by adding inter-satellite measurement data based on satellite-ground link measurements, high-precision combined orbit determination and time synchronization can be realized. What is more, orbit and time synchronization can be maintained to realize autonomous orbit determination and time synchronization even without ground station support. At the same time, the communication capability can be used to realize the global transmission of remote control and telemetry, real-time update of navigation messages, and other services data.

Some scholars have conducted research on joint orbit determination and autonomous orbit determination in recent years. However, most of these studies were experimental work carried out before the Global Navigation Satellite System (GNSS) was established [12–17]. As a result, the research findings may not fully reflect the performance of the complete system architecture [18]. During the construction of BDS-3, some scholars analyzed the orbit determination and time synchronization performance using on-orbit data.

Hu [19] conducted a performance analysis on four experimental satellites and proposed an improved algorithm for detecting and repairing cycle slips based on ionospheric delay polynomial prediction. With the increasing number of satellites, ISL data are gradually improving orbit determination accuracy. Yang [20] and Ruan [21] analyzed ISL data from 8 satellites. Ruan [21] proposed a general observation model that utilizes non-simultaneous observations directly. Data analysis revealed a root mean square value of 0.019 m for the overlapping orbit difference in the radial direction, and an overlapping clock difference of 0.185 ns (95%). However, there is a lack of orbit determination performance analysis for GEO satellites.

Achieving autonomous orbit determination and time synchronization in BDS-3 holds strategic significance. Minimizing dependence on ground stations is a crucial step toward enhancing system autonomy. The core of autonomous orbit determination and time synchronization lies in using ISL data to autonomously estimate satellite orbits and onboard clock errors, thereby maintaining the constellation ephemeris.

Currently, two processing methods can achieve this goal: centralized and distributed algorithms [22, 23]. The distinction between centralized and distributed algorithms lies in whether all parameters are estimated in a single filter or individually. In the centralized algorithm, one satellite collects all inter-satellite link measurements and utilizes them to simultaneously estimate the orbits and clock offsets of all satellites. Conversely, the distributed algorithm individually estimates satellite-related orbit and clock offsets. In the distributed algorithm, a satellite gathers only the measurements relevant to its own orbit and clock offset estimation. The centralized algorithm offers the advantage of providing an optimal solution with high accuracy. However, it comes with the drawback of requiring extensive computation and being impractical for on-board execution. On the other hand, the distributed algorithm requires less computation and is suitable for on-board execution, but it provides a suboptimal solution with lower accuracy.

Tang [15, 22] conducted centralized autonomous orbit determination and time synchronization experiments and proposed a method for deriving satellite clock offset without loss of accuracy. The simulation results indicate that the radial overlap difference of autonomous orbits for IGSO satellites is less than 15.0 cm, and for MEO satellites, it is less

than 10.0 cm. Song [24] independently determined the orbits of three experimental satellites using the least squares estimation algorithm, and the error in the radial direction is less than 0.5 m. Cheng [25] proposed a givens-gentleman orthogonal transformation method without square root calculations to conduct centralized autonomous orbit determination analysis on 18 MEO satellites. Additionally, Lin [26] designed a network-wide centralized orbit determination algorithm using the generalized Kalman Filter (KF) algorithm. After optimization, the average User Range Error (URE) of the entire network of satellites is only 0.18 m.

In centralized algorithms, Guo [12] assessed the effectiveness of the proposed extended KF using 30 days of ISL data from 18 MEO satellites. Wen [23] introduced a balanced extended KF algorithm for distributed orbit determination. However, the current study relies on simulated data rather than actual on-orbit ISL data. Only by employing in-orbit data can we accurately evaluate the performance of BDS-3's autonomous orbit determination and set the groundwork for future algorithm enhancements.

The main contributions of this article can be summarized as follows:

1. It presents a well-defined global operation and service architecture for the regional stations and Ka-band ISL implemented by the BDS-3.
2. It introduces the methodology of the BDS-3 and analyzes its performance from three perspectives: joint orbit determination and time synchronization, autonomous orbit determination and time synchronization, and global service.
3. The performance improvement of the BDS-3 MEO satellite, particularly the advantages of its key technology Ka-band ISL, has been emphasized when compared to its predecessor, BDS-2. Moreover, comparative analysis with other GNSSs underscores BDS-3's superior capabilities in achieving high-precision orbit determination and time synchronization, even without globally distributed stations.
4. In the future, an integrated satellite-ground network will be established utilizing advanced laser ISL technology. This advancement will enable higher precision measurements and increased data transmission bandwidth, comprehensively enhancing time synchronization, autonomous orbit determination and time synchronization, and global service performance.

The main contents of this article are as follows: First, it introduces the operational and service architecture of the BDS-3, which is based on regional ground stations and ISL. Additionally, it presents joint and autonomous orbit determination and time synchronization methods. Subsequently, on-orbit data results are calculated. Based on this, the characteristics and performance of global data transmission are analyzed. Moreover, the performance of other GNSSs is evaluated and compared in the discussion, and the future development trend of the Beidou system is proposed. Finally, conclusions are drawn.

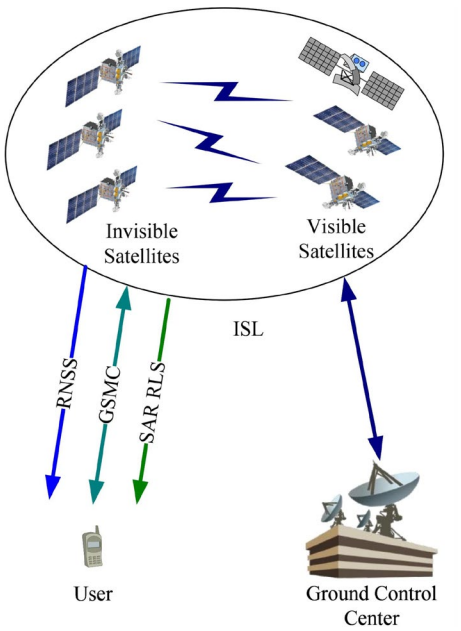

Fig. 1 Operations and services architecture

2 Operations and services architecture

The architecture of the BDS-3 system consists of three parts, which include the ISL network, regional ground control center, and global users. The architecture is shown in Fig. 1.

2.1 System components

The nodes of the ISL network are composed of 30 satellites in three hybrid orbits: GEO, MEO and IGSO. Three GEO satellites are located at 80° E, 110.5° E, and 140° E, respectively. The MEO constellation adopts Walker 24/3/1 configuration, with an orbit height of 21,528 km, an orbit inclination of 55° and zero eccentricity. The IGSO orbit comprises three satellites with a phase difference of 120°, an inclination of 55° and an ascending intersection longitude of 118°. Each satellite is equipped with a Ka-band ISL payload, which can establish links between satellites and provide high-precision inter-satellite measurement and efficient data transmission. Moreover, global RNSS, Global Short Message Communication (GSMC), Search And Rescue (SAR), and Return Link Service (RLS) services are supported, and the functions such as space-time benchmark, constellation management, and autonomous orbit determination and time synchronization can also be realized [27–29].

The regional ground control center mainly manages and operates the satellites, including commanding data upload, online fault monitoring and fault diagnosis, resource management and scheduling, and performance evaluation. The satellite-ground network can not only distribute the global service-related data to the whole constellation, but also receive the telemetry and other status data of the satellites of the whole constellation. Theoretically, establishing only one ground station to realize global operations and services is reasonable.

The users of BDS-3 are composed of various types of handhelds, on-board, and shipborne terminals with global RNSS, GSMC, SAR, and RLS services.

2.2 Working mode

The architecture has two operating modes. One is the conventional working mode. When the satellite-ground network is in a normal working state, the precise orbit determination and time synchronization are realized through the inter-satellite and satellite-ground measurement values. And the navigation messages, GSMC, SAR, RLS, and remote-control related data are uploaded into the visible satellite and distributed to the invisible satellite through ISL to provide high-quality services for all kinds of users. The other is the autonomous working mode. When the ground control center is unavailable, BDS-3 uses the ISL network instead to provide services for users over a period of time. The inter-satellite measurements are used for autonomous orbit determination and time synchronization. And those parameters are broadcasted to users by downlink signals.

3 Combined orbit determination and time synchronization

The measurement between BDS-3 satellites in Ka-band is an observation independent of ground stations, which provides additional and important observation data for enhancing the solution of BDS-3 satellite orbit determination and time synchronization.

3.1 Calculation method

Assuming that the satellite i obtains the inter-satellite observation $P_{i,j}(t_{i,j})$ of the satellite i at $t_{i,j}$ time, the observation equation can be expressed as follows [15],

$$P_{i,j}(t_{i,j}) = \left\| R_i(t_{i,j}) - R_j(t_{i,j} - \tau_{i,j}) \right\| + \delta_i(t_{i,j}) - \delta_j(t_{i,j} - \tau_{i,j}) + \Delta_j + \beta_i + \omega, \quad (1)$$

where $\tau_{i,j}$ is the time of signal propagation in space, R_i and R_j are the satellite positions of signal reception and transmission, respectively. δ_i and δ_j are the clock error of satellite i and j, respectively. Δ_j and β_i are the hardware delay of

Table 1 Strategies of combined orbit determination

Arc length	3 Days
Observations	Geometric distances from ISL two-way measurements, code and carrier phase measurements from six regional monitoring stations
Weight	Code:ISL:Phase=1:100:10,000
Estimated solar parameters	Bias in D direction, Y direction and B directions, cosine and Sine parameters in the B direction
Troposphere delay factor	One parameter per 2 h
Clock offsets	Clock offsets of the master station is fixed as known values, clock offsets of the satellites and other receivers are estimated as white noise
Solar radiation pressure	ECOM 5 model

transmitting and receiving equipment, respectively, which usually have good stability and can be regarded as a constant in a short time (such as a few days). ω is the measurement noise. It is worth mentioning that Eq. (1) omits the correction terms such as relativistic delay of signal propagation and phase center deviation of satellite antenna.

Because the BDS-3 satellite is equipped with a high-stable atomic clock, the satellite clock error changes linearly in a short time. The two-way observations of satellite *i* and satellite *j* are converted to the same time by using the predicted orbit and clock error parameters respectively, then added to eliminate the satellite clock error parameters, and obtain the instantaneous geometric distance, which only includes the satellite orbit parameters. The processing strategy of combined inter-satellite link observations and ground station observations is shown in Table 1.

The inter-satellite geometric distance obtained above and the satellite-ground pseudo-range and phase data measured by the ground monitoring stations of the regional network are combined for orbit determination. In the combined orbit determination process, the normal equation is constructed using satellite-ground and ISL observation data and then superimposed to obtain the final normal equation. Finally, the least squares method is used to estimate the optimal solution of the satellite orbit. The above process has been applied to calculate the broadcast ephemeris of the BDS-3 satellites.

3.2 Performance analysis

Based on the data of seven days from August 29, 2021, to September 5, 2021, the BDS-3 space signal accuracy in navigation messages is analyzed. The broadcast ephemeris is compared with the precision orbit and clock error calculated by the IGS MGEX Analysis Center. Because polynomial parameters are used to filter the ISL measurements, the residuals can be considered as measurement noise. As shown in Fig. 2, the Root Mean Square (RMS) of the filtered residuals for 24 MEO satellites is given. It is not difficult to see that the RMS of the filtered residuals for each MEO satellite is less than 3 cm. Additionally, illustrated in Figs. 3 and 4, exemplified by the M1 and M9 satellites, the error sequence of the ISL for three days is presented to characterize the level of inter-satellite measurement noise. It can be observed that the ISL error sequence exhibits significant random fluctuations. It can be seen that the quality of Ka ISL observation data is guaranteed.

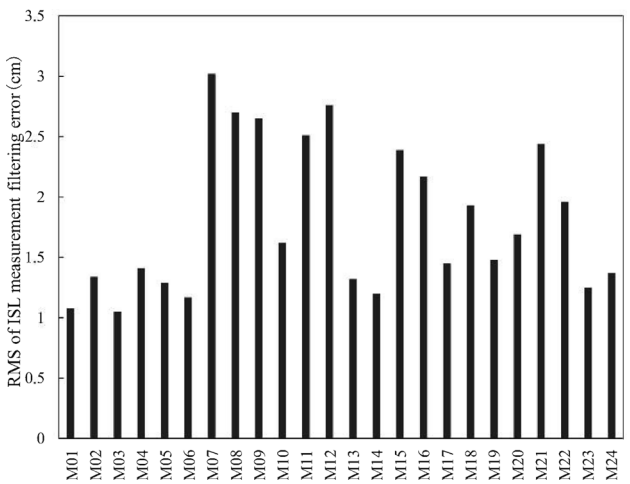

Fig. 2 The RMS of the filtering residuals for each satellite

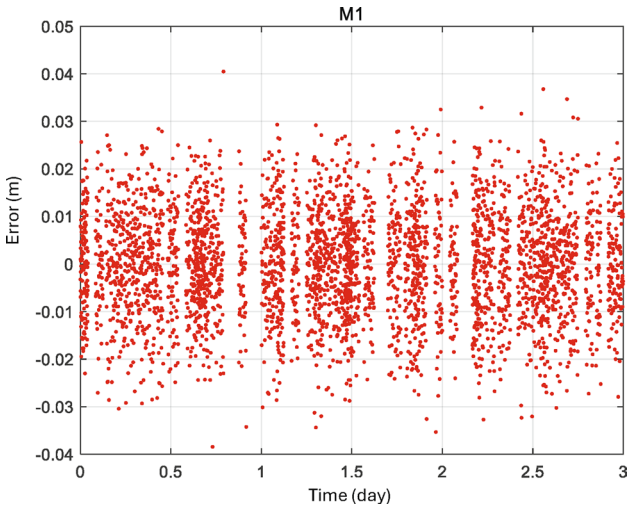

Fig. 3 ISL Measurement noise error sequence of the M1 satellite over three days

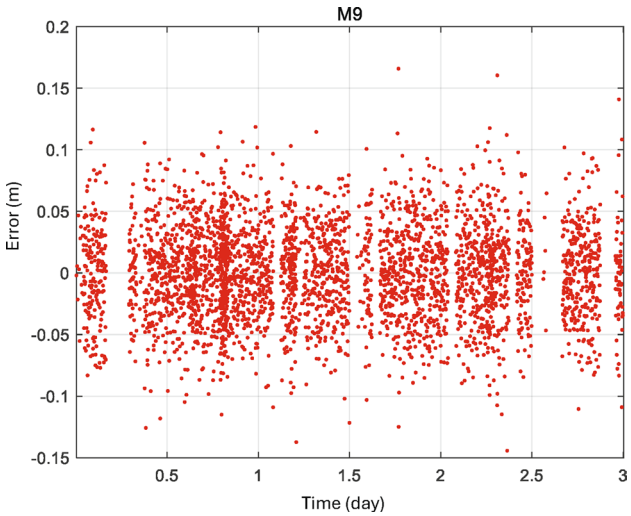

Fig. 4 ISL Measurement noise error sequence of the M9 satellite over three days

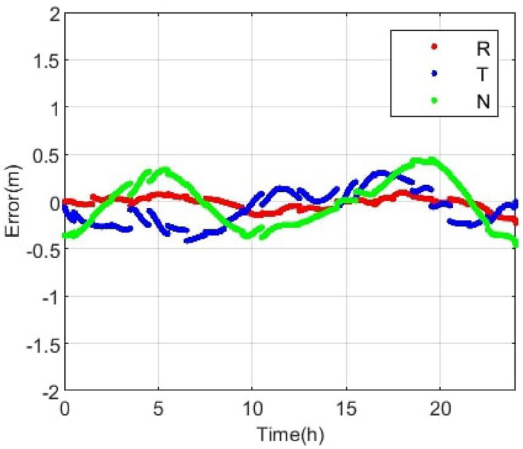

Fig. 5 RTN error of M12 (BDS-3)

Furthermore, as shown in Figs. 5, 6, 7, 8, taking the data on September 2, 2021 as an example, the orbit and clock error of every BDS-3 satellite in one day are analyzed to obtain the orbit error in R (Radial), T (Tangential), N (Normal) directions, URE and clock error.

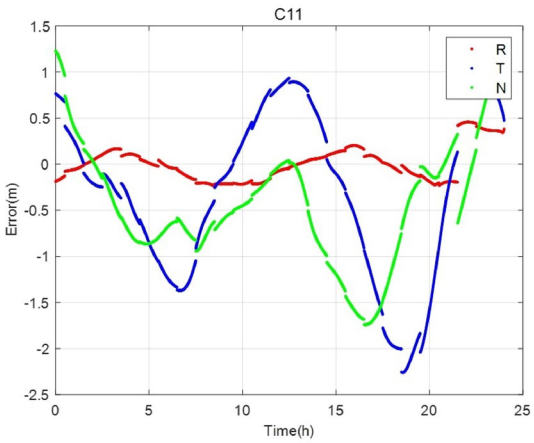

Fig. 6 RTN error of M03 (BDS-2)

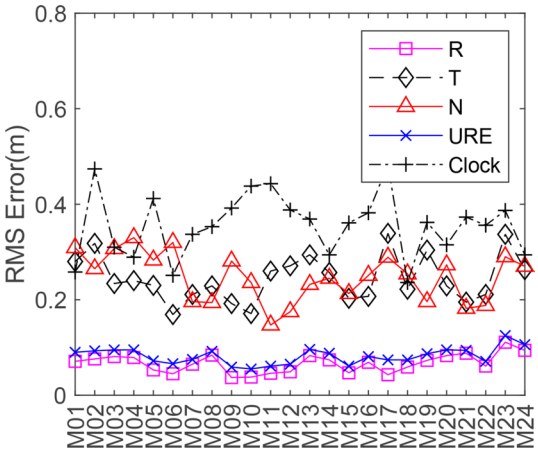

Fig. 7 Error results of different BDS-3 MEO satellites (R, T, N, URE, and Clock error)

Figure 5 shows the RTN error curve of broadcast ephemeris for M12 in one day, which has the characteristics of a typical BDS-3 MEO satellite. It can be seen that the absolute value of orbit error in R, T and N directions does not exceed 0.5 m and has a certain periodicity. The deviation in the R direction is the smallest and the most stable, and the RMS value is less than 0.1 m. Compared with the RTN error of the BDS-2 M03 satellite (as shown in Fig. 6), the errors in T and R directions of the BDS-3 M12 satellite are significantly less than those of the BDS-2 M03 satellite.

The summary of orbit and clock error of all MEO satellites in the BDS-3 constellation is shown in Fig. 7. The orbit radial error of the BDS-3 satellite constellation can be seen as generally better than 0.1 m. The error of each satellite in the R, T, and N directions is not greater than 0.5 m, and the URE value is not more than 0.2 m. In addition, the error of the BDS-3 satellite clock error parameter is about 0.3−0.5 m.

Table 2 Comparison of research results (combined orbit determination)

Literature	OD Result/cm *				TS Result/ns *	Number of satellite	GS & OT*
	Satellite	3D RMS	Radial	URE			
[29]	MEO	50	–	–	–	8	GS
[21]	MEO	15.6	1.9	–	0.185	8	GS
[30]	MEO	15.4	–	–	–	18	GS
[31]	MEO	–	4.1	–	–	15	GS
This paper	IGSO	–	6.7	8.2	1.16	28	OT
	MEO	–	10	11.9			
	GEO	–	44.4	46.5			

* OD and TS represent Orbit Determination and Time Synchronization, respectively. GS and OT represent Ground Simulation and On-board Test, respectively

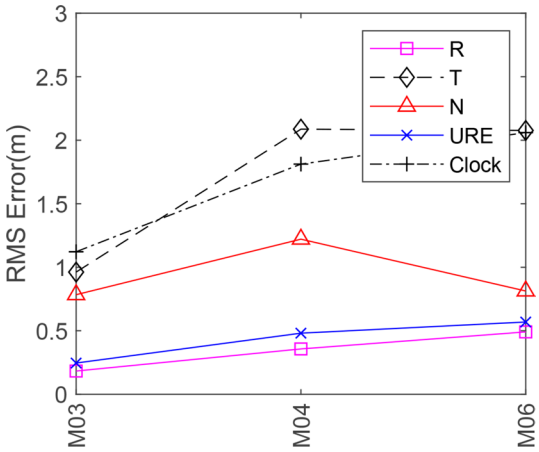

Fig. 8 Error results of different BDS-2 MEO satellites (R, T, N, URE, and Clock error)

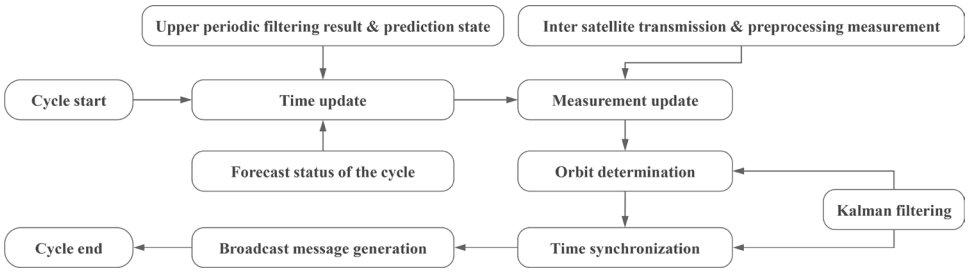

Fig. 9 Autonomous orbit determination and time synchronization process of each cycle

The comparison with other literature research results is shown in Table 2. Clearly, our analysis results may not seem remarkable when compared to existing studies. This is primarily because our assessment is grounded in joint orbit determination and time synchronization results derived from measurements taken by 28 operational satellites. In contrast, other studies commonly employ software simulations or ground-based algorithm simulations, utilizing only a portion of the spaceborne ISL data. In addition, other research results mainly focus on evaluating MEO satellites, and we supplement the orbit determination results of GEO satellites and IGSO satellites. Among the three types of satellites, the orbit determination accuracy of IGSO satellites is better than that of MEO and GEO. In terms of clock error, there is still room for considerable improvement. Therefore, the accuracy of the BDS-3 satellite space signal can be further improved by improving the clock error accuracy.

Figure 8 shows the summary of orbit and clock error of three MEO satellites in the BDS-2 constellation. The orbital radial error of the MEO satellite of BDS-2 is less than 0.5 m, the average errors in T and N directions exceed 1 m. The URE value is more than 0.2 m, and the clock error is about 1–2 m.

Overall, the BDS-3 on-orbit operation results demonstrate the effectiveness of the proposed architecture. As depicted in Figs. 7 and 8, in comparison to BDS-2, the orbit determination accuracy of BDS-3 has improved from 0.6 m to 0.15 m, and the time synchronization accuracy of BDS-3 has improved from 6.67 ns to 1.16 ns.

4 Autonomous orbit determination and time synchronization

Under normal circumstances, the ground station summarizes the ranging values of domestic and offshore satellites for high-precision positioning and time determination, then generates navigation messages to be broadcast by each satellite. When the ground station can't work normally, developing high-precision autonomous orbit determination and time synchronization is vital to the continuity and stability of global services.

4.1 Calculation method

A set of distributed algorithms based on the long-term prediction ephemeris is studied. After using each cycle's ranging value for preprocessing, Kalman filter technology is used for real-time orbit determination and time synchronization. The process of each cycle is shown in Fig. 9.

The state quantity of orbit determination Kalman filter for each satellite is six parameters $X = \left(x, y, z, v_x, v_y, v_z\right)$ of the satellite's position and velocity. In the process, ΔX participates in the calculation due to the demand for linearization.

The time update performs one-step extrapolation based on the long-term prediction ephemeris to complete the time update for the orbit information, so as to obtain the orbit estimation value of the current cycle, and calculates the state transition matrix, as shown in Eq. (2), (3) and (4),

$$X_{k/k-1} = \Phi^*_{k,k-1}(X_{k-1} - X^*_{k-1}) + X^*_k, \tag{2}$$

$$\Phi_{k,k-1} = f(X_{k/k-1}, X_{k-1}), \tag{3}$$

$$P_{k/k-1} = \Phi_{k,k-1} P_{k-1} \Phi^{\mathrm{T}}_{k,k-1} + Q_{k-1}, \tag{4}$$

where $\Phi^*{}_{k,k-1}$ is the state transition matrix based on the long-term ephemeris, X^*_{k-1} and X^*_k are the long-term ephemerides, $\Phi_{k,k-1}$ is the state transition matrix based on the predicted value, P_{k-1} is the covariance of the state quantity of the previous period, and Q_{k-1} is the noise covariance of the state transition process. $P_{k/k-1}$ corresponds to the predicted state quantity $\hat{X}_{k/k-1}$ covariance.

After preprocessing, the measurement update uses the ISL observation to modify the predicted state quantity to obtain the measurement update state quantity. The original pseudo-range measurements obtained from the ISL contain various measurement errors, which need to be preprocessed. As shown in Table 3 [32], the preprocessing of the original measurement data mainly includes outlier elimination, epoch conversion, tropospheric error calculation, relativistic effect correction calculation, antenna phase center correction, etc. Specifically, the anti-difference filtering design algorithm is employed to address outliers [33]. Its fundamental concept involves dynamically adjusting the weight of the observation value based on the residual of the measurement value and the inspection threshold. This aims to decrease the influence of measurement values with significant errors and eliminate outliers. The processed two-way ranging value is shown in Eq. (5) [18],

$$\begin{cases} \rho_{ji} = \rho^0_{ji} + c(\delta t^i(t_r^{ji}) - \delta t^j(t_t^{ji})) + c\delta\tau^j_t + \\ \qquad c\delta\tau^i_r + I_{troji} + I_{relji} + I^i_{rp} + I^j_{tp} + \varepsilon_{ji} \\ \rho_{ij} = \rho^0_{ij} + c(\delta t^j(t_r^{ij}) - \delta t^i(t_t^{ij})) + c\delta\tau^i_t + \\ \qquad c\delta\tau^j_r + I_{troij} + I_{relij} + I^j_{rp} + I^i_{tp} + \varepsilon_{ij} \end{cases}, \tag{5}$$

where ρ^0_{ji} and ρ^0_{ij} represent the distance between the satellite centroids, $\delta t^i(t_r^{ji})$, $\delta t^j(t_t^{ji})$, $\delta t^j(t_r^{ij})$, and $\delta t^i(t_t^{ij})$ represent the clock error at each time of the satellite, $\delta\tau^i_r$, $\delta\tau^i_t$, $\delta\tau^j_r$, and $\delta\tau^j_t$ represent the satellite transceiver channel delay, I_{troji} and I_{troij} represent the tropospheric error, I_{relji} and I_{relij} represent the theory of relativity effect correction, I^i_{rp}, I^i_{tp}, I^j_{rp}, and I^j_{tp} indicate phase center correction. After correction, ρ^0_{ij} and ρ^0_{ji} are obtained, as shown in Eq. (6),

$$\frac{\rho^0_{ji} + \rho^0_{ij}}{2} = \left|X_i - X_j\right|, \tag{6}$$

where X_i is the state quantity to be estimated of the local satellite, which can be calculated by ephemeris message. After linearizing $\left|X_i - X_j\right|$, the measurement equation is obtained, as shown in Eq. (7),

$$\Delta Z_k = H_k \Delta X_k + V_k, \tag{7}$$

where ΔZ_k is the measurement residual, H_k is the measurement matrix, V_k is the measurement noise, and the measurement noise covariance is R. Then the filter gain is:

Table 3 The error model of inter-satellite observation pseudo-range and its preprocessing method

Symbol	Physical Meaning	Characteristic	Pretreatment Method
ρ_{ji}, ρ_{ij}	Pseudo range observations	Affected by various factors, outliers may occur with a certain probability.	Outlier elimination
ρ_{ji}^{0}, ρ_{ij}^{0}	Distance between satellite centroid	Contains the orbit data to be solved for autonomous orbit determination and time synchronization, which is the position at the time of sending and receiving of ranging.	Pseudo-range reduction
$\delta t^{i}\left(t_{r}^{ji}\right)$, $\delta t^{j}\left(t_{j}^{ji}\right)$ $\delta t^{j}\left(t_{r}^{ij}\right)$ $\delta t^{i}\left(t_{t}^{ij}\right)$,	The satellite clock error of each time	Contains the clock error data to be solved for autonomous orbit determination and time synchronization, which is the ranging time clock error for sending and receiving.	Pseudo-range reduction
$\delta\tau_{r}^{i}$,$\delta\tau_{t}^{i}$,$\delta\tau_{r}^{j}$,$\delta\tau_{t}^{j}$	Satellite transceiver channel delay	It is a constant error within a certain time.	Pre-calibration method
I_{mulji},I_{mulij}	Multipath error	There are few occludes in the satellite space environment, and the multipath error is very small.	Ignore
I_{troji},I_{troij}	Tropospheric error	Most links do not pass through the troposphere, and the troposphere delay of ISLs is not considered.	Ignore
I_{ionji},I_{ionij}	Ionospheric error	Most links do not pass through the ionosphere, and the ionospheric delay of the inter-satellite link is not considered.	Ignore
I_{relji},I_{relij}	Relativistic effect correction	Calculated from the position velocity of the link-building satellite.	According to the error model calculation
I_{rp}^{i},I_{tp}^{i},I_{rp}^{j},I_{tp}^{j}	Phase Center Correction	Calculated by satellite attitude, antenna installation parameters, beam pointing.	According to the error model calculation

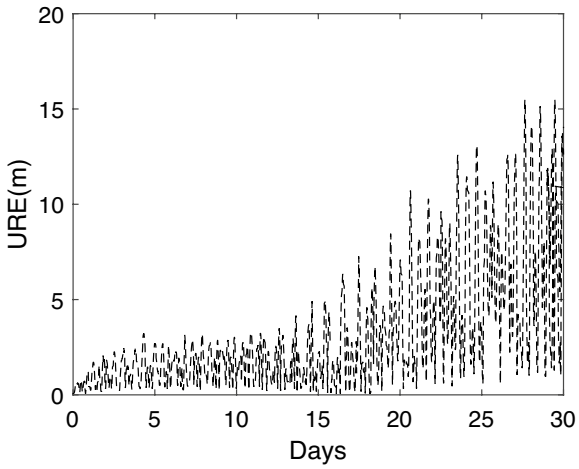

Fig. 10 The 30-day results of URE

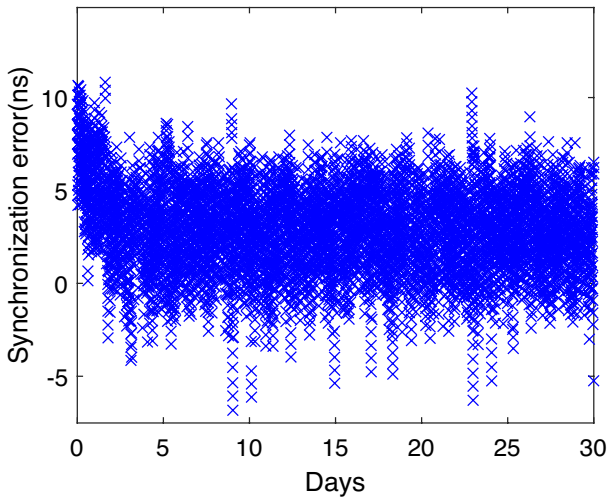

Fig. 11 The 30-day results of autonomous time synchronization

$$K_k = P_{k/k-1}H_k^{\mathrm{T}}(H_k P_{k/k-1}H_k^{\mathrm{T}} + R_k)^{-1}, \tag{8}$$

where H_k and V_k contain the information of each used link.

$$X_k = X_{k/k-1} + K_k(\Delta Z_k - H_k \Delta X_{k/k-1}), \tag{9}$$

$$P_k = (I - K_k H_k)P_{k/k-1}, \tag{10}$$

The principle of time-synchronized Kalman filter is the same as that of orbit determination, except that the filtered state quantity is set as the secondary fitting parameter of satellite clock error prediction, $X_{clk} = (a_0, a_1, a_2)$, and the state transition matrix is shown in Eq. (11).

$$\Phi_{clk} = \begin{bmatrix} 1 & T & T^2 \\ 0 & 1 & 2\times T \\ 0 & 0 & 1 \end{bmatrix}, \tag{11}$$

In the measurement equation, $\frac{\rho_{ij}^0 - \rho_{ji}^0}{2c} = X_{iclk} - X_{jclk}$, where X_{jclk} is calculated by ephemeris message.

Table 4 Comparison of research results (autonomous orbit determination)

Literatur	Mode*	OD Result/cm *			TS Result/ns *	Number of Satellite	Total/day	GS & OT*
		Satellite	Radial	URE				
[22]	C	Experimental	10	–	–	5	10	GS
[15]	C	IGSO	≤15	–	0.2	4	18	GS
		MEO	≤10	–				
[24]	C	Experimental	≤50	–	–	3	5	GS
[25]	C	MEO	–	≤50	≤1	18	30	GS
[26]	C	MEO	–	≤18	–	24	30	GS
[12]	D	MEO	19	–	–	18	30	GS
[23]	D	MEO	–	–	–	24	7	GS
This paper	D	MEO	–	779	2.97	24	30	OT

* C and D represent Centralized and Distributed algorithms, respectively. OD and TS represent Orbit Determination and Time Synchronization, respectively. GS and OT represent Ground Simulation and On-board Test, respectively

4.2 Performance analysis

Based on the above algorithms and measured data, a 30-day autonomous orbit determination and time synchronization test of 24 MEO satellites is completed. Taking one MEO satellite as an example, the results are shown in Figs. 10 and 11. It can be seen that the peak URE value of autonomous orbit determination within 30 days is 16 m, with an average of 7.9 m. The 30-day time synchronization error RMS is 3.74 ns, with an average of 2.97 ns.

Table 4 is a comparison with other literature research results. It is not difficult to find that the centralized autonomous algorithm has better autonomous orbit determination results than the distributed one. However, the centralized algorithm poses a more significant challenge to the computing and storage resources of in-orbit satellites.

In order to further support this argument, we can analyze it from two perspectives of computing resources and communication resources. First of all, in terms of communication resources, the distributed scheme only requires the transmission of the two-way pseudo-range to the link-building satellite. In contrast, the centralized scheme requires all satellites to transmit the pseudo-range to the main satellite. Considering that the number of satellites in the entire network is S, each satellite having an average of 10 visible satellites, the distributed scheme needs to generate $S \times 10 \times 2$ transmission frames for the inter-satellite network. Additionally, after the main satellite completes its calculations, the results of each satellite need to be distributed, generating further inter-satellite frames. This increases the communication pressure on the inter-satellite network.

Regarding computing resources, the distributed scheme processes data from an average of 10 satellites, resulting in a maximum matrix dimension of 10×10. In contrast, the centralized algorithm requires the main satellite to process data from all network satellites, leading to a maximum matrix dimension of $S \times S$. This significantly burdens the main satellite computationally and diminishes the system's reliability.

Hence, the distributed algorithm is more suitable for the satellite's onboard operating conditions. Although the existing distributed algorithms have shown good performance, they all analyze the collected ISL data through ground simulation, not the actual on-orbit operation results. Therefore, we truly evaluate the performance of BDS-3's autonomous orbit determination through 30 days of on-orbit measurements.

5 Global data transmission

In order to support global operations and services, BDS-3 needs to support diversified data transmission types. However, because the satellite of BDS-3 is equipped with only one Ka-band antenna, the satellite network is discontinuous in its connectivity, and only ISLs switch among different time slots to realize the interconnection among the satellite network. Therefore, the navigation satellite network is a typical Delay/disruption-Tolerant Networks (DTN) [34]. The performance of the DTN network is closely related to the outcomes of inter-satellite link planning. Thus, the quality of

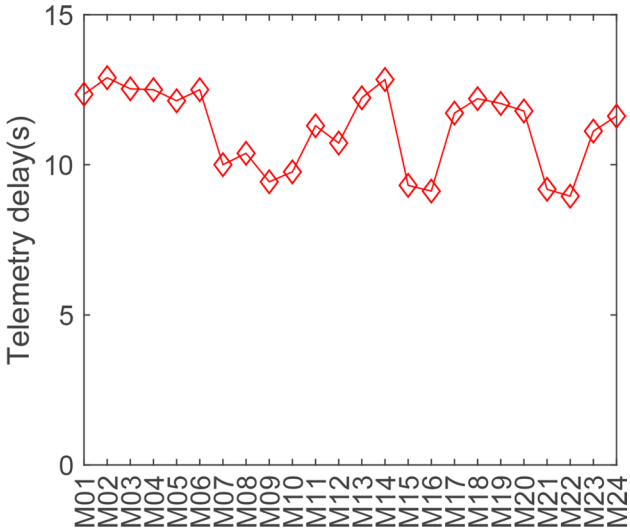

Fig. 12 Statistical results of telemetry delay of BDS-3 satellites

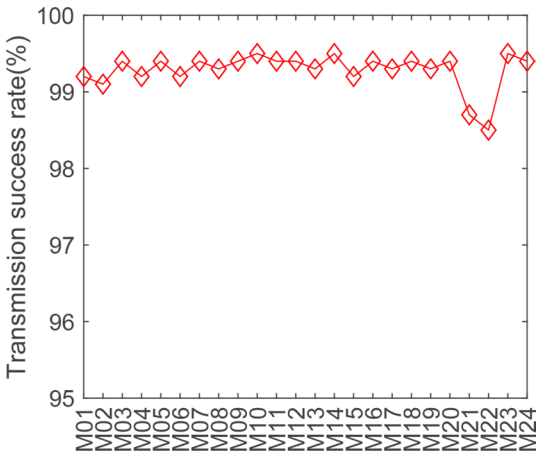

Fig. 13 Success rate of telemetry data transmission of BDS-3 satellites

BDS-3's inter-satellite link topology planning and the communication performance of the network can be assessed by examining the service transmission performance.

5.1 Date transmission type

Inter-satellite measurement data exchange needs to be carried out regularly to support periodic high-precision orbit determination and time synchronization. In terms of navigation, message transmission needs to be updated regularly to enable users to obtain orbit and clock error parameters that meet the system standards for business services. In remote control and telemetry data transmission, it involves remote control parameters and load state change parameters, which have certain randomness. In terms of GSMC and RLS data transmission, it is necessary to send relevant data to users in almost real-time because it involves search and rescue related information.

On the data transmission path, different from the traditional inter-satellite communication network, the inter-satellite data transmission characteristic of BDS-3 is not the data transmission between any two satellite nodes in the network. However, it mainly focuses on the two-way data interaction between visible and invisible satellites of regional ground stations, including remote control and message data sent by regional ground stations to invisible satellites to ensure that the ground station can control the satellite in almost real-time and update messages. The telemetry data is transmitted from the invisible satellite to the regional ground station to ensure that the regional ground station can monitor the status of the invisible satellite. It also includes that the regional ground station sends search and rescue-related information to invisible satellites.

The most data transmission scenarios are data transmission between regional stations and invisible global MEO satellites. By optimizing the topology and routing design, the data transmission performance of the delay-tolerant network supporting BDS-3 global operations and services can be significantly improved.

Table 5 Performance comparison of four GNSSs

OD result/cm	Radial				TS result/ns
	Satellite	GEO	IGSO	MEO	
Four GNSSs	BDS-3	44	6.7	10	1.16
	GPS	–	–	59	1.8
	GLONASS	–	–	123	7.55
	Galileo	–	–	19	1.05

5.2 Performance analysis

Taking telemetry parameters transmission as an example, the measured data from 00:00 on October 18, 2021 to 00:00 on October 24, 2021 (Beijing time) for a total of 6 days are counted. Figures 12 and 13 show the statistical results of telemetry delay and success rate of different BDS-3 MEO satellites for telemetry data transmission. Among them, the maximum delay of the MEO satellite is 12.90 s, the average delay is 11.19 s, and the overall data transmission success rate is better than 99%.

6 Discussion

The BDS-3 system was officially launched on July 31, 2020, providing all-weather, all-time, high-precision positioning, navigation, and timing services to users worldwide. At the same time, other satellite navigation systems have also entered a new stage of development. On December 19, 2018, the United States launched a new generation of GPS III navigation satellites to improve system performance. After stagnation, GLONASS actively transitioned its mechanism from frequency division multiple access to code division multiple access. Galileo has met initial operational capability since December 15, 2016, and is rapidly progressing toward full operational capability [35]. Therefore, it is vital to conduct an in-depth investigation and analysis of the performance of BDS-3 and compare it with other satellite navigation systems.

The performance [36] of the four major navigation systems in terms of orbit determination accuracy and time synchronization is in Table 5. In the R direction, the MEO satellite of BDS-3 is significantly better than other navigation systems. However, Galileo has the best performance in time synchronization, and BDS-3 is relatively poor.

Therefore, in the development of the next-generation navigation system, the Beidou system will initiate the primary enhancement in its system architecture [37]. This advancement involves the integration of high-precision laser ISL terminals, paving the way for the creation of an integrated high-precision measurement and big data bandwidth Positioning, Navigation, and Timing (PNT) network [38] in satellite-ground communications. The introduction of laser terminals ensures a higher level of accuracy in measurement data, thereby enhancing the system's joint orbit determination and optimizing time synchronization accuracy. Additionally, bolstering the computing resources of satellites will effortlessly resolve complex challenges related to centralized autonomous orbit determination. Simultaneously, the high-speed transmission capability of lasers will significantly augment the system's communication performance.

7 Conclusion

The architecture based on regional ground stations and ISL has been applied to the BDS-3 project and efficiently solved the problem of global operations and services. Since the BDS-3 system was built more than a year ago, the architecture has operated stably and effectively supported the realization of global functions and performance indicators. The strong support of the architecture makes BDS-3 a high-precision and diversified-service GNSS. In the future, the Beidou system will continue enhancing its system architecture and performance, aiming to establish a more robust and comprehensive PNT network. This development will enable the creation of higher-precision spatio-temporal benchmarks, ensuring greater accuracy and reliability in navigation and positioning technologies.

Author contributions Conceptualization, GL and SG; methodology, WG, KH., FS, CT, and FZ; investigation, GL, KH, and WW; writing-original draft preparation, GL and KH; writing-review and editing, SG, WG, and WG; supervision, SG and WG. All authors have read and agreed to the published version of the manuscript.

Funding Not applicable.

Data availability The datasets used and/or analysed during the current study are available from the corresponding author on reasonable request.

Declarations

Competing interests The authors declare that they have no Conflict of interest.

References

1. Kaplan ED, Hegarty C. Understanding GPS/GNSS: principles and applications. Boston, MA: Artech House; 2017.
2. Luba O, Boyd L, Gower A, Crum J. GPS III system operations concepts. IEEE Aerosp Electron Syst Mag. 2005;20(1):10–8. https://doi.org/10.1109/MAES.2005.1396789.
3. Maine K, Anderson P, Bayuk F. Communication architecture for GPS III. In: 2004 IEEE aerospace conference proceedings (IEEE Cat. No.04TH8720), vol 3, p 1539 (2004). https://doi.org/10.1109/AERO.2004.1367927
4. Teunissen PJ, Montenbruck O. Springer handbook of global navigation satellite systems, vol 10. Perth: Springer; 2017. https://doi.org/10.1007/978-3-319-42928-1
5. Trautenberg HL, Weber T, Schäfer C. GALILEO system overview. Acta Astronautica. 2004;55(3–9):643–7. https://doi.org/10.1016/j.actaastro.2004.05.046.
6. Abusali P, Tapley B, Schutz B. Autonomous navigation of global positioning system satellites using cross-link measurements. J Guid Control Dyn. 1998;21(2):321–7. https://doi.org/10.2514/2.4238.
7. Ignatovich E, Schekutjev A. Results of imitating tests of some versions of onboard algorithms for SC glonass intersatellite measurement processing. In: Jubilee 15th Saint Petersburg International Conference on Integrated Navigation Systems, pp 348–354; 2008. https://elibrary.ru/item.asp?id=23975046
8. Maine KP, Anderson P, Langer J. Crosslinks for the next-generation GPS. In: 2003 IEEE Aerospace Conference Proceedings (Cat. No. 03TH8652), vol. 4, pp. 1589–1596; 2003. https://doi.org/10.1109/AERO.2003.1235087 . IEEE
9. Rajan JA, Orr M, Wang P. On-orbit validation of GPS IIR autonomous navigation. In: Proceedings of the 59th Annual Meeting of The Institute of Navigation and CIGTF 22nd Guidance Test Symposium (2003), pp 411–419; 2003. https://www.ion.org/publications/abstract.cfm?articleID=3874
10. Poliak J, Calvo RM, Surof J, Richerzhagen M, Wolf R. Laboratory demonstrator of optical inter-satellite links for the Kepler system. In: Proceedings of the 31st International Technical Meeting of the Satellite Division of The Institute of Navigation (ION GNSS+ 2018), pp 861–867; 2018. https://doi.org/10.33012/2018.15886
11. Wolf R, Surof J, Poliak J, Blümel L, Agazzi L, Calvo RM. Communication and ranging system for the kepler laboratory demonstration. In: Proceedings of the 33rd International Technical Meeting of the Satellite Division of the Institute of Navigation (ION GNSS+ 2020), pp 1200–1208; 2020. https://doi.org/10.33012/2020.17615
12. Guo L, Wang F, Gong X, Sang J, Liu W, Zhang W. Initial results of distributed autonomous orbit determination for Beidou BDS-3 satellites based on inter-satellite link measurements. GPS Solut. 2020;24(3):1–11. https://doi.org/10.1007/s10291-020-00985-0.
13. Li Z, Xin J, Guo R, Li X, Tang C. Tian Y feasibility analysis of autonomous orbit determination of BDS satellites with inter-satellite links. Geomat Inf Sci Wuhan Univ. 2022;47(1):55–60. https://doi.org/10.13203/j.whugis20190338.
14. Pan J, Hu X, Zhou S, Tang C, Guo R, Zhu L, Tang G, Hu G. Time synchronization of new-generation BDS satellites using inter-satellite link measurements. Adv Space Res. 2018;61(1):145–53. https://doi.org/10.1016/j.asr.2017.10.004.
15. Tang C, Hu X, Zhou S, Liu L, Pan J, Chen L, Guo R, Zhu L, Hu G, Li X, He F, Zhiqiao C. Initial results of centralized autonomous orbit determination of the new-generation BDS satellites with inter-satellite link measurements. J Geodesy. 2018;92(10):1155–69. https://doi.org/10.1007/s00190-018-1113-7.
16. Wang C, Zhao Q, Guo J, Liu J, Chen G. The contribution of intersatellite links to BDS-3 orbit determination: model refinement and comparisons. Navigat J Inst Navigat. 2019;66(1):71–82. https://doi.org/10.1002/navi.295.
17. Yang D, Yang J, Li G, Zhou Y, Tang C. Globalization highlight: orbit determination using Beidou inter-satellite ranging measurements. GPS Solut. 2017;21(3):1395–404. https://doi.org/10.1007/s10291-017-0626-5.
18. Yang Y, Yang Y, Hu X, Tang C, Guo R, Zhou Z, Xu J, Pan J, Su M. BeiDou-3 broadcast clock estimation by integration of observations of regional tracking stations and inter-satellite links. GPS Solut. 2021;25(2):1–12. https://doi.org/10.1007/s10291-020-01067-x.

19. Hu C, Wang Q, Wang Z, Hernandez Moraleda A. New-generation Beidou (BDS-3) experimental satellite precise orbit determination with an improved cycle-slip detection and repair algorithm. Sensors. 2018;18(5):1402. https://doi.org/10.3390/s18051402.
20. Yang Y, Yang Y, Hu X, Chen J, Guo R, Tang C, Zhou S, Zhao L, Xu J. Inter-satellite link enhanced orbit determination for BeiDou-3. J Navigat. 2020;73(1):115–30. https://doi.org/10.1017/S0373463319000523.
21. Ruan R, Jia X, Feng L, Zhu J, Huyan Z, Li J, Wei Z. Orbit determination and time synchronization for BDS-3 satellites with raw inter-satellite link ranging observations. Satell Navigat. 2020;1(1):1–12. https://doi.org/10.1186/s43020-020-0008-y.
22. Tang C, Hu X, Zhou S, Pan J, Guo R, Hu G, Zhu L, Li X, Wu S, Wang Y. Centralized autonomous orbit determination of Beidou navigation satellites with inter-satellite link measurements: preliminary results. Sci Sin-Phys Mech Astron. 2017;47(2):95–105. https://doi.org/10.1360/SSPMA2016-00355.
23. Wen Y, Zhu J, Gong Y, Wang Q, He X. Distributed orbit determination for global navigation satellite system with inter-satellite link. Sensors. 2019;19(5):1031. https://doi.org/10.3390/s19051031.
24. Song X, Mao Y, Feng L, Jia X, Ji j. The Preliminary Result an Analysis for BD Orbit Determination with Inter-satellite Link Data. Acta Geodaetica et Cartographica Sinica. 2017;46(5):547–53. https://doi.org/10.11947/j.AGCS.2017.20160203.
25. Cheng J. Research on centralized autonomous orbit determination key technology with Beidou-3 inter-satellite link ranging. Wuhan University, Wuhan, China. https://www.cnki.net/kns/defaultresult/index
26. Lin X, Lin B, Liu Y, Bai T, Wu G, Wang Z. Research on centralized autonomous orbit determination algorithm for Beidou satellites. J Jilin Univ (Inf Sci Ed). 2020;38(4):428–32. https://doi.org/10.19292/j.cnki.jdxxp.2020.04.007.
27. Li G, Guo S, Lv J, Zhao K, He Z. Introduction to global short message communication service of BeiDou-3 navigation satellite system. Adv Space Res. 2021;67(5):1701–8. https://doi.org/10.1016/j.asr.2020.12.011.
28. Li G, Guo S, He Z, Gao Y, Li W. BDS-3 SAR service and initial performance. GPS Solut. 2021;25(4):1–8. https://doi.org/10.1007/s10291-021-01170-7.
29. Yang Y, Gao W, Guo S, Mao Y, Yang Y. Introduction to BeiDou-3 navigation satellite system. Navigat J Inst Navigat. 2019;66(1):7–18. https://doi.org/10.1002/navi.291.
30. Yang Y, Yang Y, Hu X, Tang C, Zhao L, Xu J. Comparison and analysis of two orbit determination methods for BDS-3 satellites. Acta Geodaetica et Cartographica Sinica. 2019;48(7):831. https://doi.org/10.11947/j.AGCS.2019.20180560.
31. Zhang R, Tu R, Zhang P, Fan L, Han J, Lu X. Orbit determination of BDS-3 satellite based on regional ground tracking station and inter-satellite link observations. Adv Space Res. 2021;67(12):4011–24. https://doi.org/10.1016/j.asr.2021.02.027.
32. Chang J. The error analysis and optimization of the autonomous navigation algorithm of navigation satellites. Shanghai Institute of Microsystem and Information Technology, University of Chinese Academy of Sciences, Shanghai, China (2018). https://d.wanfangdata.com.cn/thesis/ChJUaGVzaXNOZXdTMjAyNDAxMDkSCFkzNTA5MzA4Ggg3N2thb2o3dw%3D%3D
33. Xu B, Yang X, Hou W, Li Y. An Outlier-Rejection Single Observation Passive Locating Algorithm Based on M-Estimators. Radar Sci Technol. 2016;14(6):599–604. https://doi.org/10.3969/j.issn.1672-2337.2016.06.008.
34. Han K, Xu B, Shao F, Gong W, Ren Q, Chang J. An adaptive topology optimization strategy for intersatellite links in GNSS. IEEE Trans Aerosp Electron Syst. 2022;58(6):5894–907. https://doi.org/10.1109/TAES.2022.3181555.
35. Montenbruck O, Steigenberger P, Hauschild A. Comparing the 'Big 4'-A User's View on GNSS Performance. In: 2020 IEEE/ION Position, Location and Navigation Symposium (PLANS), pp 407–418; 2020. https://doi.org/10.1109/PLANS46316.2020.9110208. IEEE
36. Liu W, Liu J, Xie J, Jiao B. Signal-in-Space Range Error of the Global BeiDou Navigation Satellite System and Comparison with GPS, GLONASS, Galileo, and QZSS. J Surv Eng. 2023;149(1):04022013. https://doi.org/10.1061/(ASCE)SU.1943-5428.0000413.
37. Yang Y, Ren X, Jia X, Sun B. Development trends of the national secure PNT system based on BDS. Sci China Earth Sci. 2023;1:1–10. https://doi.org/10.1007/s11430-022-1069-7.
38. Yang Y, Yang C, Xia R. PNT intelligent services. Acta Geodaetica et Cartographica Sinica. 2021;50(8):1006. https://doi.org/10.11947/j.AGCS.2021.